

# Discrete modeling of plastic cement paste subjected to drying

V. Slowik

Leipzig University of Applied Sciences, Leipzig, Germany

J. W. Ju

University of California, Los Angeles, USA

**ABSTRACT:** Prior to initial setting, cement paste may be regarded as a suspension consisting of solid particles and water. Drying leads to a curved water surface in the spaces between the solid particles at the specimen boundary. A negative capillary pressure is built up which results in shrinkage strain and, possibly, in cracking. The concept of discrete modeling has been used for simulating these processes. In 2D models consisting of circular solid particles and a liquid phase, the drying induced capillary pressure build-up and the corresponding particle displacements are simulated. Under certain conditions, crack initiation due to capillary forces may be observed. The simulations allow the demonstration of different influences on capillary shrinkage cracking.

## 1 INTRODUCTION

The present work aims at the modeling of drying induced concrete cracking in the very early age; i.e., within approximately four hours after casting when the material is still in its plastic stage. In this early age, the hardening process has not yet led to a significant tensile strength of the material. The predominant reason for volume changes and cracking are physical phenomena rather than the beginning chemical reactions. The latter are not decisive for the material behavior in this age, although they do have an influence.

In the following, the material behavior of a drying suspension is described. The corresponding physical processes may be observed in cement paste before initial setting as well as in drying suspensions with inert solid particles.

After the material has been placed in a mould, the solid particles tend to settle due to their self-weight. That is, water is transported to the upper surface. If the water content of the system is high enough, a plane water film is formed on top of the near-surface particles; Figure 1(A). This process is also referred to as bleeding.

Evaporation at an open surface and in the case of cement paste also self-desiccation lead to the loss of water from the system. If the solid near-surface particles are no longer covered by a plane water film, the water surface will be curved. In the interparticle spaces, menisci are formed; see Figure 1(B). Accordingly, a capillary pressure is built up in the water phase (Wittmann 1976, Radocea 1992). Although

this pressure is lower than the pressure of the surrounding air, it will be considered as a positive quantity in the following discussion.

The capillary pressure results in inward forces acting on the particles at the specimen face where evaporation takes place. As a consequence, shrinkage deformations may be observed, the so-called capillary shrinkage. For cementitious materials, the term plastic shrinkage is also used since this deformation is taking place in the plastic stage.

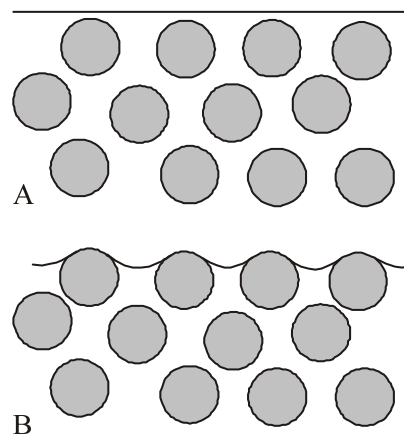


Figure 1. Surface of a drying suspension. Plane water film covering the solid particles at the surface (A) and formation of menisci in the interparticle spaces (B).

In the beginning of the capillary pressure build-up, only vertical shrinkage strain may be observed; i.e., deformation in the direction perpendicular to the open surface. Later, the material might crack or separate from the side faces of the mould. This al-

lows for horizontal shrinkage strain. The volume change of the drying material is in this stage almost equal to the volume of the evaporating water.

If a certain material specific pressure is reached, not all the interparticle spaces at the surface of the drying suspension can be bridged by the menisci anymore. Air penetrates locally into the system, forming weak spots at the surface and allowing crack initiation. It has been shown by electron microscopic observations (Schmidt et al. 2007, Slowik et al. 2008a) and force measurements (Slowik et al. 2008b) that the local air entry is a precondition for crack formation in the plastic concrete. However, air entry does not necessarily result in cracks since sufficient particle mobility is also a precondition.

The capillary pressure reached at the first event of air entry is referred to as air entry value. The latter is a material parameter of the suspension and may be identified in laboratory experiments (Slowik et al. 2008a).

If the capillary pressure in a drying suspension is always lower than the air entry value, cracking is prevented. This is because crack initiation requires air entry. On this basis, a concept of controlled concrete curing in the plastic material stage has been proposed (Schmidt et al. 2007, Slowik et al. 2008a). The capillary pressure build-up in plastic cementitious materials appears to be reversible (Wittmann 1976). Hence, it is possible to decrease the capillary pressure by rewetting the surface. Figure 2 shows the capillary pressure versus time in a cement paste sample. When a predefined threshold of 15 kPa had been reached, the sample was shortly rewetted by dispersing fog above the surface. Only a few seconds of rewetting were required for a significant temporary reduction of the pressure. The rewetting was terminated after the pressure had reached a certain lower limit. It is not advisable to reduce the capillary pressure down to zero since, in that case, a plane water film would be created on the surface which might degrade the surface properties of the hardened material. The closed-loop control allows to keep the capillary pressure within an uncritical range; i.e., between certain predefined limits.

It has been demonstrated that the capillary pressure controlled rewetting of the surface is possible under site conditions and that, in this way, the cracking risk in the plastic stage may be reduced significantly (Slowik et al. 2008b). The method requires an in situ capillary pressure measurement which is possible by using wireless sensors (Schmidt et al. 2009). For rewetting the surface, commercially available fogging devices may be utilized. It has to be pointed out that water supply from the concrete surface requires sufficient permeability of the material. This condition is fulfilled in ordinary plastic concrete. However, if the loss of water is predominantly caused by self-desiccation at a later age, rewetting of

the surface might be ineffective since the water will not penetrate the material having already a reduced permeability. Under such conditions, internal curing might be an appropriate method.

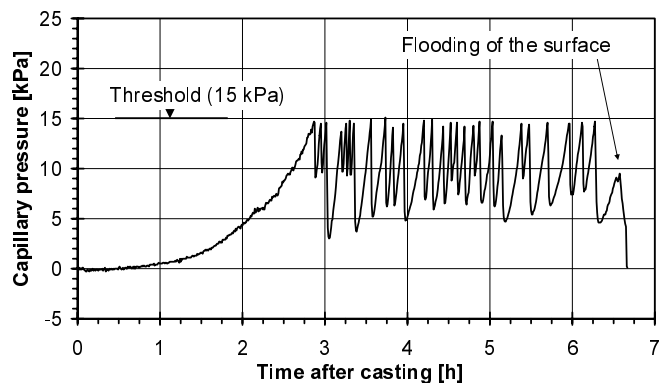


Figure 2. Capillary pressure versus time during controlled curing of a cement paste sample. The surface of the sample has been rewetted after the threshold value had been reached.

The method of controlled concrete curing requires the identification of a critical capillary pressure which should not be exceeded while the concrete is in its plastic stage. As mentioned before, this threshold should be lower than the material's air entry value. The latter may be determined experimentally and depends on particle content and size distribution as well as on the mobility of the particles. In order to obtain a better understanding of the processes leading to air entry and crack initiation, numerical simulations are performed. Possibly, the simulation results will also allow us to identify the critical capillary pressure of a certain material and to estimate the early age cracking risk.

## 2 DESCRIPTION OF THE MODEL

### 2.1 Generation of the initial particle structure and simulation of drying

To simulate the characteristic material behavior of suspensions subjected to drying, the concept of discrete modeling appears to be appropriate. 2D particle models with circular solid grains were generated. The grains represent cementitious or inert particles of a drying suspension. They are dispersed in a liquid phase which represents the water.

For the generation of the initial particle structure, a stochastic-heuristic algorithm is adopted, which was originally developed for concrete meso-level models (Leite et al. 2007). The particles are placed in the sample one after the other according to size starting with the largest one. Firstly, the respective particle is placed at a random position. If it overlaps previously allocated particles or the specimen

boundaries, it is moved in order to resolve the conflict. If no acceptable position has been found after several translational movements, a new random position is tested. This algorithm permits us to obtain considerably higher particle contents than those achievable by a purely stochastic procedure.

Drying is simulated by reducing the water content in a rectangular specimen (Slowik et al. 2009). The top face of the corresponding specimen is assumed to be open; i.e., evaporation may take place. The other three faces of the specimen are considered to be in contact with the mould. Initially, all particles are completely covered by the water. Then, water loss is simulated by incrementally increasing the capillary pressure and calculating the course of the water front under the assumption of constant curvature according to the respective pressure value. Despite the limitation of the model to two dimensions, axi-symmetric pores were assumed; i.e., the water menisci were considered to be double-curved forming a spherical surface. Hence, the radius of curvature of the liquid surface is calculated by

$$r = \frac{2\gamma}{p} \quad (1)$$

where  $r$  = radius of curvature;  $\gamma$  = surface tension of the liquid; and  $p$  = absolute value of the capillary pressure.

For the calculation of the water loss, however, cylindrical menisci in the water front as well as cylindrical solid particles are assumed. The different assumptions concerning the particle shape were made in order to allow a realistic modeling in spite of the two-dimensionality.

## 2.2 Forces acting on the solid particles

The solid particles are subjected to the following types of forces:

- Gravitational forces
- Forces resulting from capillary pressure
- Intermolecular forces

Gravitational forces are calculated under the assumption of spherical particles. Buoyancy in the liquid phase is taken into account.

The capillary pressure results in inward forces acting on those particles which are not completely surrounded by water; see Figure 3. For the calculation of these resultants, spherical particles are assumed as in the case of gravitational forces.

Between neighboring grains, interparticle forces are considered; see Figure 3. They include both the electrostatic and the van-der-Waals force. By superposition, a resulting force is obtained, see Figure 4. The van-der-Waals force is always attractive between particles of the same material and describes the interac-

tion of electrically neutral particles. The electrostatic force describes the repulsion of the ion clouds which are surrounding solid particles in an aqueous solution. The resulting force, see Figure 4, is characterized by repulsion in the short-distance range and by attraction at larger particle distances. At the equilibrium particle distance, the value of the resulting force is zero. The magnitude of the interparticle forces depends on the properties of the solid particles as well as on the properties of the surrounding liquid. Details of the model assumptions concerning interparticle forces are given by Slowik et al. (2009).

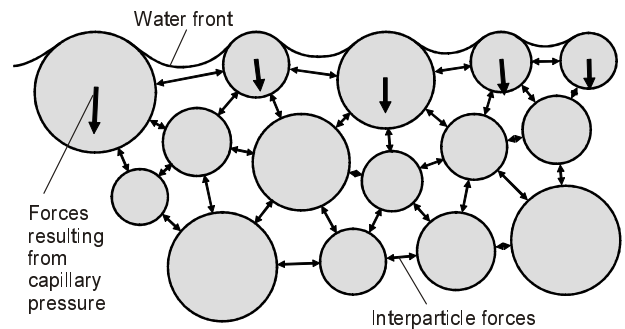


Figure 3. Forces acting on the solid particles. Gravitational forces are not shown.

It has to be pointed out that for the interparticle force in the short-distance and overlapping range, a parabolic function has been adopted which was not directly derived from physical considerations (Slowik et al. 2009). This function has to meet certain requirements of the numerical solution method and may be regarded as a penalty force function which prevents the particle from overlapping and direct contact. In reality, solvation forces and the Born repulsion are acting in the short-distance range. These forces are considered to be included in the above mentioned parabolic function.

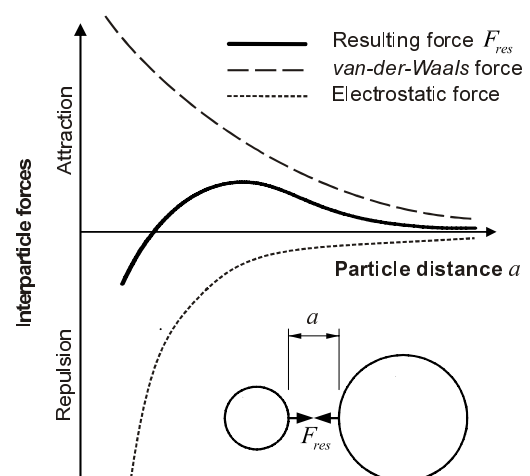


Figure 4. Intermolecular forces versus particle distance (not to scale).

Frictional forces are not considered since the solid particles do not have direct contact. Further-

more, viscosity of the liquid phase and inertia are disregarded since the drying induced particle movement is comparably slow.

The physical properties of the solid and liquid phase are kept constant during the simulations. This means, all influences of the cement hydration are disregarded. The modeled material may be considered as a suspension made of inert solid particles and water. Experimental results have shown that in drying suspensions with fly ash the same effects as in plastic cement paste may be observed (Slowik et al. 2008a).

For the considered type of material, the equilibrium particle distance; i.e., the distance at zero inter-particle force, see Figure 4, amounts to a few nanometers. In a 2D model, however, a larger equilibrium particle distance has to be assumed. The 2D model represents a section through a 3D sample. The shortest connecting lines between neighboring particles lie not necessarily within this section. Therefore, the apparent particle distances in the 2D section are larger than in the spatial particle structure. For the simulations presented here, the equilibrium particle distance was adjusted so that the particle content in the unloaded model is equal to the one in the real material (Slowik et al. 2009). The standard value used here was 1.5  $\mu\text{m}$ .

### 2.3 Solution method

Previously published simulation results were obtained by using an implicit solution scheme (Slowik et al. 2009). This type of analysis is based on an imaginary truss model the members of which were the connecting lines between neighboring particles. The latter were considered to be the joints of the truss. Forces resulting from capillary pressure as well as gravitational forces are acting on these imaginary joints. By an iterative matrix stiffness method, a state of equilibrium is searched. In each of the iterations, the connectivities between the particles are updated and a new water front is calculated. The particle displacements in each iteration are the solution of a linear system of equations:

$$\frac{d\Pi(\Delta_1, \dots, \Delta_i, \dots, \Delta_n)}{d\Delta_i} = \frac{d(W_{int} - W_{ext})}{d\Delta_i} = 0 \quad (2)$$

where  $\Pi$  = potential energy of the system;  $W_{int}$  and  $W_{ext}$  = internal and external work, respectively;  $\Delta_i$  = displacement at degree of freedom  $i$ ; and  $n$  = number of degrees of freedom. In this way, the particles are shifted towards directions which minimize the potential energy of the system.

For determining the internal portion of the potential energy, the secant slope of the force-distance curve, see Figure 4, serves as “member” stiffness. When previously set convergence limits are reached,

the next load step is applied; i.e., the next capillary pressure increment. The convergence criteria are based on particle displacements and unbalanced forces. When no water front connecting the side faces of the mould can be found anymore or a further pressure increase does not yield physically sound results, the simulation is terminated.

In order to reduce the computing time for the simulations, an explicit solution scheme was to be tested as an alternative to the previously described method. Another reason for this was the poor convergence behavior of the implicit solution in the case of larger models. The application of an explicit algorithm was expected to allow a larger particle number in the simulations.

The applied explicit solution scheme is based on the Distinct Element Method (DEM). For consecutive time steps, the acceleration of the particles is calculated:

$$\ddot{u} = \frac{F}{m} = \frac{F_e}{m} + g \quad (3)$$

where  $u$  = displacement of the respective particle;  $F$  = sum of forces acting on the particle;  $F_e$  = sum of forces acting on the particle without gravitational force;  $m$  = mass of the particle; and  $g$  = gravitational acceleration. Forces, displacements and accelerations are vectors.

On the basis of the acceleration, the velocity and the displacement of the respective particle are calculated by using the central difference method. In order to ensure numerical stability as well as computational efficiency, the length of the time step was adjusted according to the current maximum stiffness:

$$\Delta t = 2\beta \cdot \sqrt{\frac{m_{min}}{k_{max}}} ; 0 \leq \beta \leq 1 \quad (4)$$

where  $\Delta t$  = time step;  $m_{min}$  = minimum particle mass in the system; and  $k_{max}$  = maximum contact stiffness in the system. The parameter  $\beta$  was usually set to 0.1.

Forces  $F$  and  $F_e$  in Eq. 3 include a damping force which is required for numerical stability. In the simulations presented here, a mass dependent damping force has been applied:

$$F_d = -\alpha m \dot{u} \quad (5)$$

where  $F_d$  = damping force;  $m$  = particle mass; and  $\alpha$  = damping factor. The latter was adjusted in a trial-and-error procedure for the particular simulations to be performed. By using an additional stiffness dependent damping force, the performance of the algorithm could not be improved.

### 3 SIMULATION RESULTS

In previous parametric studies which were performed by using the implicit solution scheme, some effects of the material composition on the behavior of drying suspensions could be shown (Slowik et al. 2009). The results presented in the following were obtained by using the above described explicit solution scheme. On the basis of the simulations performed so far, it may be concluded that with both solution schemes qualitatively the same results are obtained.

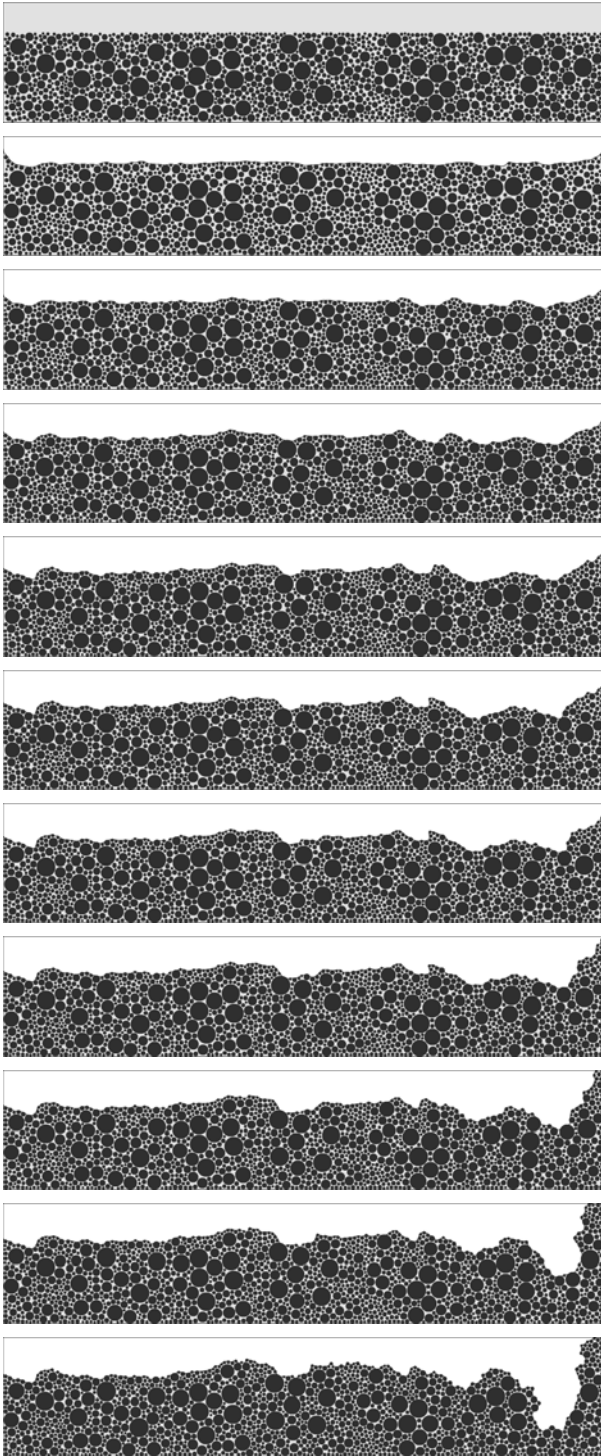


Figure 5. Simulation of the capillary pressure build-up in a drying suspension, particle sizes ranging from 4  $\mu\text{m}$  to 32  $\mu\text{m}$ , equilibrium particle distance 1.5  $\mu\text{m}$ , absolute capillary pressure values from top to bottom in kPa: 0; 12; 24; 36; 44; 46; 48; 51; 57; 61; 80 (approximate values).

Figure 5 shows a model of a drying suspension under increasing capillary pressure. In the first line; i.e., at zero pressure, the initial particle arrangement may be seen. All particles (dark circles) are below the water surface. When water (gray) is evaporating, menisci are formed in the water front between the particles at the surface and, accordingly, a capillary pressure is built up in the liquid phase. This pressure results in downward forces acting on the particles and leading to a settlement of the material. The vertical displacement of the near-surface particles appears to be non-uniform and air entry into the system does not occur everywhere at the same pressure. It may be seen that a local breach is formed at a pressure of about 57 kPa. This breach is later widened by the horizontal components of the increasing capillary pressure and the attracting interparticle forces decrease to a negligible value. This phenomenon of strain localization and separation is regarded as crack initiation.

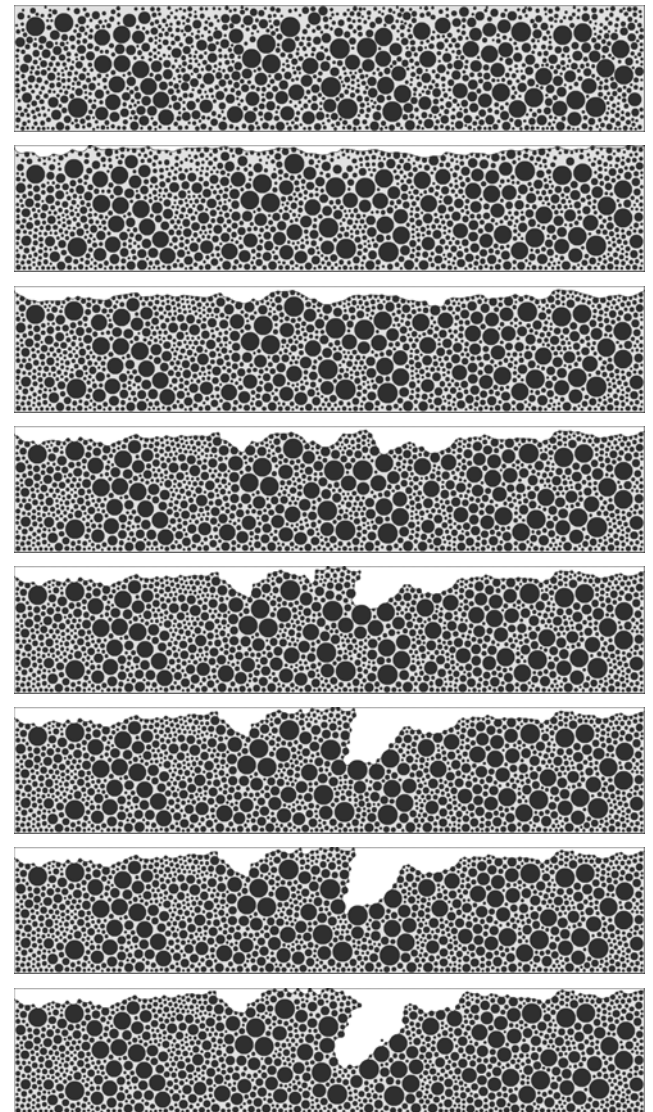


Figure 6. Simulation of the capillary pressure build-up in a drying suspension, particle sizes ranging from 4  $\mu\text{m}$  to 32  $\mu\text{m}$ , equilibrium particle distance 3  $\mu\text{m}$ , absolute capillary pressure values from top to bottom in kPa: 0; 12; 24; 36; 44; 46; 47; 49 (approximate values).

Figure 6 shows a similar simulation, however with a comparably large equilibrium particle distance of 3  $\mu\text{m}$ . For the generation of the initial particle structure, the same particle content has been used as in the case of the smaller equilibrium particle distance; see Figure 5. However, the initial minimum particle distance was larger.

Due to the increased particle mobility in the case of the large equilibrium particle distance, the air entry value; i.e., the pressure at the first event of air entry seems to be lower than in the case of the small equilibrium particle distance. This points towards a higher cracking risk. The same tendency has been found by using the implicit solution scheme (Slowik et al. 2009).

Figure 7 shows the corresponding curves of the capillary pressure versus water loss. The discontinuities in the beginning of the pressure build-up may be attributed to the rearrangement of particles.

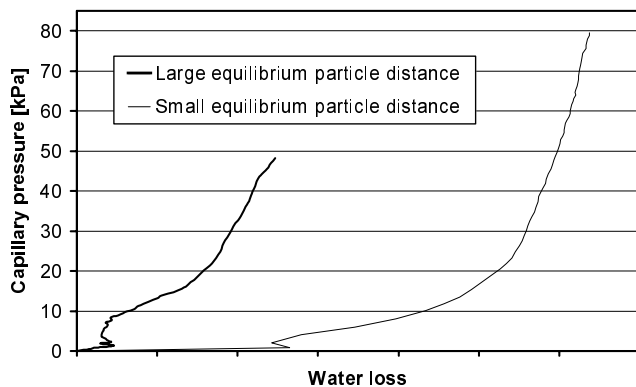


Figure 7. Capillary pressure versus water loss for the simulations presented in Figures 5 and 6, respectively.

It appears to be difficult to retrieve out of the 2D simulation results realistic water loss values which may be compared to corresponding experimentally determined values. For this reason, no numbers are assigned at the abscissa in Figure 7. The capillary pressure values, however, are in good accordance with experimental observations. It may be seen that the material with the smaller equilibrium particle distance shows a higher water loss in the beginning and a stronger consolidation under the increasing capillary pressure. When the material is consolidated, however, the slope of the curve is steeper in the case of the smaller equilibrium particle distance. This may be explained by the smaller surface pores and corresponds to experimental observations. The smaller the pores at the surface of a drying suspension, the steeper the pressure increase will be.

#### 4 CONCLUDING REMARKS

The behavior of drying suspensions has been simulated by using a discrete particle-based model. Ef-

fects like capillary pressure build-up, shrinkage and crack initiation have been demonstrated and conclusions concerning the cracking risk in plastic cement paste may be drawn.

Whereas for previously published results an implicit solution scheme has been applied, the results presented here were obtained by using the Distinct Element Method as an explicit solution scheme. The simulations performed so far with the last mentioned method confirm the previous findings.

It should be indicated that the model does not yet include age-dependent material properties and the evolution of the particle sizes due to cement hydration. However, plastic cement paste and suspensions with inert solids show a similar drying behavior.

#### ACKNOWLEDGMENT

The work of the first author was performed under a Fulbright Scholarship. This support is gratefully acknowledged.

#### REFERENCES

- Leite, J.P.B., Slowik, V. & Apel, J. 2007. Computational model of mesoscopic structure of concrete for simulation of fracture processes. *Computers and Structures* 85(17-18): 1293-1303.
- Radocea, A. 1992. A study on the mechanism of plastic shrinkage of cement-based materials. PhD thesis. Göteborg: Chalmers University of Technology Göteborg.
- Schmidt, D., Slowik, V., Schmidt, M. & Fritzsche, R. 2007. Auf Kapillardruckmessung basierende Nachbehandlung von Betonflächen im plastischen Materialzustand (Early age concrete curing based on capillary pressure measurement). *Beton- und Stahlbetonbau* 102(11): 789-796.
- Schmidt, M. & Slowik, V. 2009. Capillary shrinkage cracking and its prevention by controlled concrete curing. In K. Kovler (ed.), *Proceedings of the 2<sup>nd</sup> International RILEM Workshop on Concrete Durability and Service Life Planning – ConcreteLife'09*, Haifa, Israel, 7-9 September 2009: 23-30. Bagnex, France: RILEM Publications S.A.R.L.
- Slowik, V., Schmidt, M. & Fritzsche, R. 2008a. Capillary pressure in fresh cement-based materials and identification of the air entry value. *Cement and Concrete Composites* 30(7): 557-565.
- Slowik, V., Schmidt, M., Neumann, A. & Dorow, J. 2008b. Early age cracking and its influence on the durability of concrete structures. In T. Tanabe, K. Sakata, H. Mihashi, R. Sato, K. Maekawa, H. Nakamura (eds.), *Proceedings of the 8th International Conference on Creep, Shrinkage and Durability Mechanics of Concrete and Concrete Structures - CONCREEP 8*, Ise-Shima, Japan, 30 September – 2 October 2008: Vol. 1, 471-477. London: Taylor & Francis Group.
- Slowik, V., Hübner, T., Schmidt, M. & Villmann, B. 2009. Simulation of capillary shrinkage cracking in cement-like materials. *Cement & Concrete Composites* 31(7): 461-469.
- Wittmann, F.H. 1976. On the action of capillary pressure in fresh concrete. *Cement and Concrete Research* 6: 49-56.